0026-895X/95/050965-12$3.00/0

MOLECULAR PHARMACOLOGY, 47:965–976 (1995).

Interaction of Dolastatin 10 with Tubulin: Induction of Aggregation and Binding and Dissociation Reactions

RUOLI BAI, GEORGE F. TAYLOR, JEAN M. SCHMIDT, MICHAEL D. WILLIAMS, JOHN A. KEPLER, GEORGE R. PETTIT, and ERNEST HAMEL

Laboratory of Molecular Pharmacology, Developmental Therapeutics Program, Division of Cancer Treatment, National Cancer Institute, National Institutes of Health, Bethesda, Maryland 20892 (R.B., E.H.), Research Triangle Institute, Research Triangle Park, North Carolina 27709 (G.F.T., J.A.K.), and Cancer Research Institute, Arizona State University, Tempe, Arizona 85287 (J.M.S., M.D.W., G.R.P.)

Received October 21, 1994; Accepted February 8, 1995

SUMMARY

We have prepared [^{3}H]dolastatin 10 and examined its interactions with tubulin. Binding kinetics appeared to be biphasic, with a rapid initial reaction that could not be accurately measured, followed by a slower second reaction. Bound drug was stable in centrifugal gel filtration, column gel filtration, and high performance liquid chromatography gel filtration, but the bound drug could be displaced by an active isomer of dolastatin 10. Scatchard analysis of binding data was consistent with two classes of binding sites. However, dolastatin 10 induced an aggregation reaction upon binding to tubulin, complicating analysis of the data, and incorporation of [^{3}H]dolastatin 10 into large aggregates was readily demonstrated. The chromatographic properties of the smallest radiolabeled species that could be documented were most consistent with a complex consisting of two molecules of α/β-tubulin dimer and two molecules of [^{3}H]dolastatin 10. The coexistence of an aggregation reaction with a binding reaction at a single site probably underlies the biphasic binding kinetics and the biphasic Scatchard plot. Of peptides that strongly inhibit tubulin polymerization (dolastatin 10, dolastatin 10 isomers, segments, and analogs, dolastatin 15, and phomopsin A), only those previously shown to be strong inhibitors of vinblastine binding and nucleotide exchange also strongly inhibited [^{3}H]dolastatin 10 binding and induced tubulin aggregation (dolastatin 10 itself, two chiral isomers of dolastatin 10, and phomopsin A). The morphology of dolastatin 10-induced aggregates was compared with that of vinblastine-induced aggregates under a variety of reaction conditions. With both drugs the aggregates had a more organized appearance when microtubule-associated proteins were included in the reaction.

Dolastatin 10 (structure in Fig. 1) is a potently cytotoxic peptide originally derived from the sea hare *Dolabella auricularia*, a shell-less mollusk (1). Dolastatin 10 causes the accumulation of cells arrested in mitosis and the disappearance of intracellular microtubules, and its intracellular target is the protein tubulin, the major component of microtubules (2, 3). Salient features of the interaction of dolastatin 10 with tubulin include potent inhibition of polymerization, noncompetitive inhibition of the binding of vincristine and vinblastine to tubulin, concordant inhibition of nucleotide exchange on β-tubulin and formation of an *N,N'*-ethylenebis(iodoacetamide)-induced intra-β-tubulin cross-link between Cys-12 and either Cys-201 or Cys-211, and stabilization of the colchicine-binding activity of tubulin (2, 4–7). In addition, higher concentrations of dolastatin 10 were shown to cause the formation of nonmicrotubule polymers of tubulin plus MAPs in the presence of GTP (2, 8). These polymeric structures are morphologically similar to those formed in the presence of another antimitotic peptide, phomopsin A (8, 9), which also is a noncompetitive inhibitor of vincristine binding to tubulin (4).

In this report we describe the synthesis of dolastatin 10 radiolabeled with tritium and initial studies on its interaction with tubulin. We also further describe the dolastatin 10-induced polymerization of tubulin (a reaction we term "aggregation," to distinguish it from normal tubulin polymerization into microtubules), because this reaction significantly affects the interpretation of studies on the binding of the radiolabeled drug to the protein.

Materials and Methods

Synthesis of [^{3}H(G)]dolastatin 10. In this work NMR spectra were recorded with a Bruker/AMX-500 multinuclear Fourier transform spectrometer, equipped with a tritium/proton dual probe, a tritium E coupler, and a selective preamplifier for tritium. Radioactivity was quantitated in a liquid scintillation counter. Radioactive TLC plates were scanned with a Berthold model LB 283 linear analyzer system. HPLC was performed with a Waters model 600A dual-pump system equipped with a Schoeffel Spectroflow monitor and an IN/US-Ram radioactivity flow detector. A solution of 10 mg of dolastatin 10 in 0.4 ml of ethyl acetate, with 15 mg of 10% platinum on carbon catalyst, was exposed to 5 Ci of carrier-free $^3H_2$ gas

ABBREVIATIONS: MAP, microtubule-associated protein; MES, 4-morpholineethanesulfonate; HPLC, high performance liquid chromatography; TLC, thin layer chromatography.

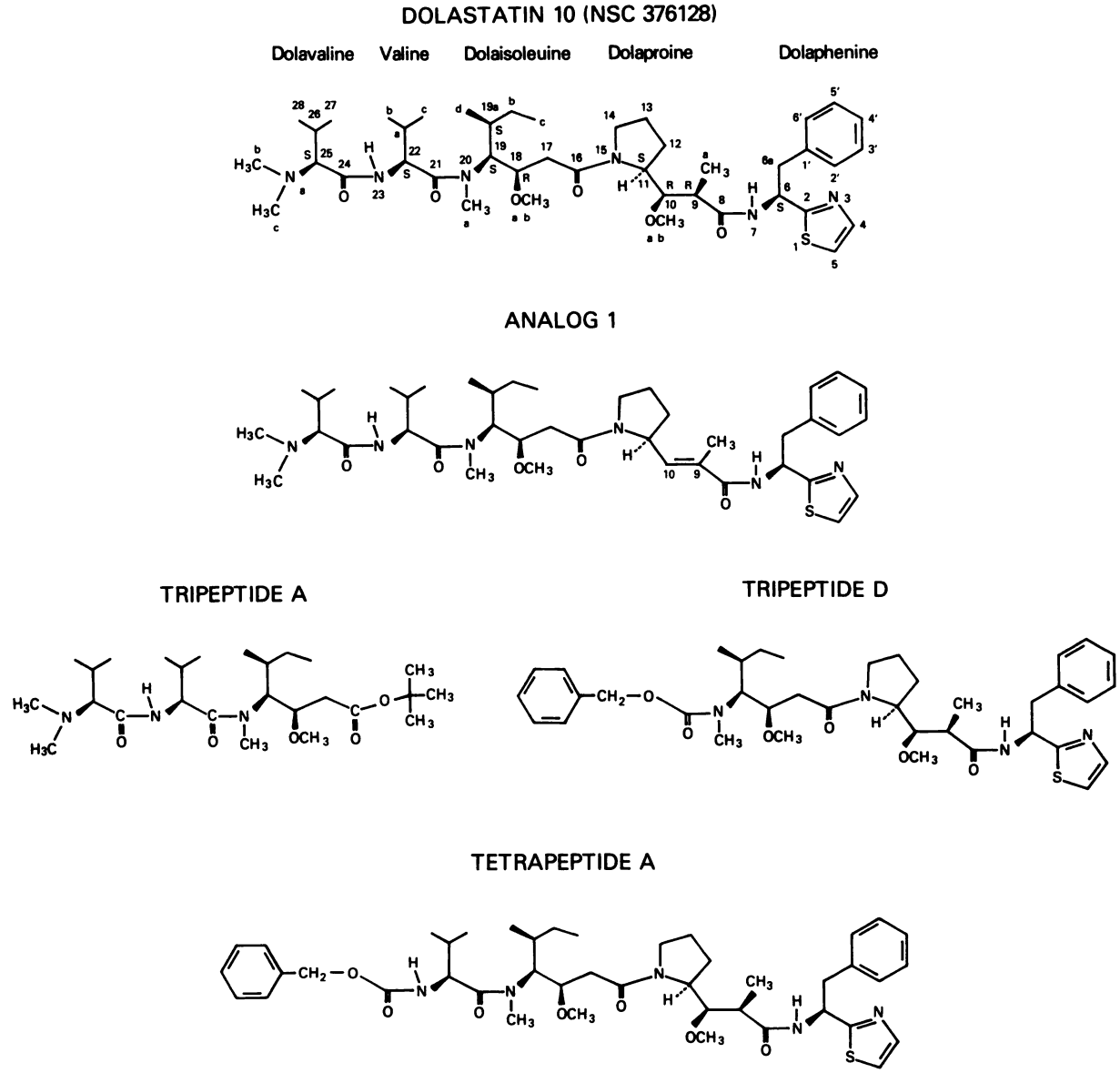

Fig. 1. Structural formulae of dolastatin 10 and related compounds.

(DuPont) for 48 hr. After removal of the catalyst by filtration, volatile components were removed by vacuum transfer, and the residue was exchanged three times with methanol. The crude material was purified by preparative TLC on a 20- × 20- × 0.025-cm silica gel plate (E. Merck) with hexane/acetone (2:3). The dolastatin 10 band was washed from the silica with $CHCl_3$/ethanol (1:1). This material showed radioactive impurities when analyzed by HPLC (DuPont Zorbax C_8, 3-μm, 0.62- × 8-cm column; solvent, methanol/water, 7:3, with 0.005 M triethylamine; flow rate, 1.0 ml/min; retention time of dolastatin 10, 11.5 min; retention time of impurities, 7.5–10 min), and it was therefore repurified by HPLC (Waters Associates Resolve C_{18} radial compression cartridge; solvent, methanol/water, 3:1, with 0.001 M triethylamine). The [^{3}H]dolastatin 10 still showed radioactive impurities, and it again underwent preparative TLC (solvent, acetone/hexane/methanol, 5:4:1). After elution from the silica as before, the [^{3}H]dolastatin 10 was 98% pure by HPLC (DuPont Zorbax Rx, 0.46- × 25-cm column; solvent, linear gradient from 25% methanol in 0.1% aqueous trifluoroacetic acid to 50% methanol in 10 min; retention time of dolastatin 10, 16.5 min) and by TLC (silica gel 60F, 5- × 20-cm analytical plate from E. Merck; solvent, acetone/hexane/methanol, 5:4:1; R_F of dolastatin 10, 0.4). The yield was 11.1 mCi, with a specific activity of 1560 Ci/mol (1.99 Ci/g). Back-exchange in phosphate buffer, pH 7, for 24 hr at room temperature showed 0.5% exchange.

The ^{1}H NMR spectrum (500 MHz, in CD_2Cl_2) of the radiolabeled material was essentially identical to that of an authentic sample. The ^{3}H NMR spectrum (533 MHz, in CD_2Cl_2) showed three signals, at δ 7.36, 7.29, and 2.22, in a ratio of 0.4:1:3. The signals at δ 7.36 and 7.29 were doublets (J = 3.7 Hz) that collapsed to singlets in the proton-decoupled spectrum. The signal at δ 2.22 was a poorly resolved multiplet that collapsed to a broad singlet in the proton-decoupled spectrum. The signals at δ 7.36 and 7.29 are assigned to the 5-position on the thiazole ring (Fig. 1), the latter based on the reported chemical shift of δ 7.25 for this proton in dolastatin 10 (1). The δ 7.36 signal is attributed to a minor conformer that was evident in the ^{1}H NMR spectra of both the radiolabeled and nonradiolabeled samples of dolastatin 10. Based on the chemical shift, the signal at δ 2.22 could be assigned to the *N,N*-dimethyl group (δ 2.26 in Ref. 1) or to the 9-position in the dolaproine residue (δ 2.28, quintet, J = 7.24 Hz, in Ref. 1). We favor assignment of this signal to the 9-position based on the method of exchange, which would be expected to effect exchange at the 9-position but not at the *N,N*-dimethyl group.

Other materials. Electrophoretically homogeneous bovine brain tubulin and heat-treated MAPs were prepared as described previously (10). Nonradiolabeled dolastatin 10, dolastatin 10 isomers and segments, and dolastatin 15 were prepared as before (7, 11, 12). Nomenclature of these structural analogs is as used previously (7, 13). Phomopsin A was a generous gift of Dr. C. C. J. Culvenor, CSIRO Division of Animal Health (Parkville, Victoria, Australia) (14).

Methods. Binding of [^{3}H]dolastatin 10 to tubulin was monitored either on columns of Sephadex G-50 (superfine), as described for individual experiments, by centrifugal gel filtration on 1.0-ml microcolumns of Sephadex G-50 (superfine) prepared in tuberculin syringes (15), or by HPLC. The standard assay conditions included 0.1 M MES (taken from a 1 M stock solution adjusted to pH 6.9 with NaOH) plus 0.5 mM $MgCl_2$. All columns and microcolumns were equilibrated with this mixture, and it was the eluting buffer. Unless otherwise indicated, the tubulin concentration was 0.25 mg/ml (2.5 μM). The drug solvent was dimethylsulfoxide, and its final concentration varied from 1 to 3% (v/v) in the individual experiments. The Lowry method was used to determine tubulin concentrations in column filtrates, for determination of the stoichiometry of drug binding. Bovine serum albumin was the protein standard.

HPLC for analysis of tubulin aggregates was performed on a TSK G3000SW column (7.5 × 300 mm), using an LKB system equipped with a Hewlett-Packard recording integrator or a Waters system equipped with a Ramona 5-LS flow detector and a Digital 380 computer.

For negative-stain electron microscopy, a 5–10-μl droplet was placed on a carbon-coated, Formavar-treated, 200-mesh, copper grid and within 10 sec was washed off with several drops of 0.5% (w/v) uranyl acetate. Excess stain was wicked off with filter paper, and grids were allowed to air dry. They were then examined with a Zeiss electron microscope. Reaction mixtures contained components described in the individual experiments, and each reaction mixture was incubated first for 15 min at room temperature (about 23°) and then for 20 min at 37°. Grids were prepared from each sample after both incubation steps, and in no case with drug was a major morphological difference observed by electron microscopy between specimens on grids prepared from the two samplings.

Results

Binding of dolastatin 10 to tubulin. In initial studies we found that centrifugal gel filtration was useful for evaluating the binding of [^{3}H]dolastatin 10 to tubulin, and we found that interaction of drug with protein was rapid. The chief practical limitations of the centrifugal gel filtration technique are, first, that there is no well defined method for stopping a reaction and, second, that this technique does not truly measure an equilibrium, because protein and ligand are separated during the procedure. Nevertheless, attempts were made to control the speed of the dolastatin 10 binding reaction by lowering the concentrations of reaction components and the reaction temperature, but these efforts were not successful.

Fig. 2 presents data from two experiments with 2.5 μM tubulin and 0.2 μM dolastatin 10 (the lowest practical concentrations for obtaining reliable measurements of protein and radioactivity in the column filtrates; note that the maximal theoretical stoichiometry for this condition would be 0.08 mol of dolastatin 10 bound/mol of tubulin). In one experiment the reaction mixture was incubated at 37° for the indicated times, and an aliquot was applied to a 37° microcolumn and immediately centrifuged. For the time 0 point, an aliquot was taken from the reaction mixture on ice and applied to a 37° column. In the second experiment the incubation was on ice and the microcolumns were processed at 4°. The time 0 aliquot was processed immediately after the last component was added to the reaction mixture.

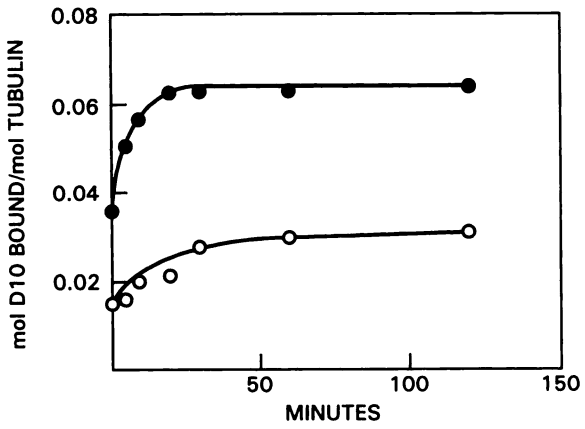

Fig. 2. Time course of binding of [^{3}H]dolastatin 10 (*D10*) to tubulin. Reaction mixtures contained 0.2 μM [^{3}H]dolastatin 10. ●, The reaction mixture was incubated at 37°. At the indicated times, duplicate 0.15-ml aliquots were placed on microcolumns warmed to 37°, and centrifugal gel filtration was immediately performed at room temperature. At time 0 the aliquots were taken from the cold reaction mixture and placed on the warm microcolumn after addition of the last component (the radiolabeled drug). ○, The reaction mixture was incubated on ice. At the indicated times, duplicate 0.15-ml aliquots were placed on microcolumns at 4°, and centrifugal gel filtration was immediately performed at 4°. At time 0 the aliquots were placed on the cold microcolumn immediately after addition of the last component. Each value represents the average of two experiments.

From these data it appears that the binding reaction is biphasic, with a significant portion of the more rapid reaction occurring so fast that initial rates cannot be measured by this technique. In addition, apparent maximal binding differs at the two temperatures. At the lower temperature, the value obtained at the initial time point was 20–25% of the theoretical maximum of 0.08 mol of drug bound/mol of tubulin. This rose slowly over the next 30 min to about twice the initial value, reaching an apparent plateau far below the final value observed at 37°. It should be noted that this could be due, at least in part, to denaturation of the tubulin, because the protein has limited stability in 0.1 M MES. In the 37° experiment, simply putting the sample on the warm microcolumn resulted in approximately twice as much drug being bound to tubulin at the initial time point. There was an additional, relatively slow, increase in binding over the next 20 min, so that the stoichiometry at the reaction plateau was about 80% of the theoretical maximum.

The biphasic reaction kinetics could have a number of explanations. They could partially originate from drug dissociation during the centrifugal gel filtration procedure, but this is unlikely (see below). Different isotypes of tubulin could have differing affinities for dolastatin 10, as has been shown for colchicine (16). Most likely, however, the biphasic binding kinetics are probably derived in large part from the aggregation reaction induced by dolastatin 10. We observed previously, although high concentrations of dolastatin 10 were used, that turbidity increased slowly over time (4). This aggregation reaction is discussed in further detail below.

Binding of [^{3}H]dolastatin 10 to tubulin was next studied over a wider range of drug concentrations at room temperature (23°), and a Scatchard analysis of the data was per-

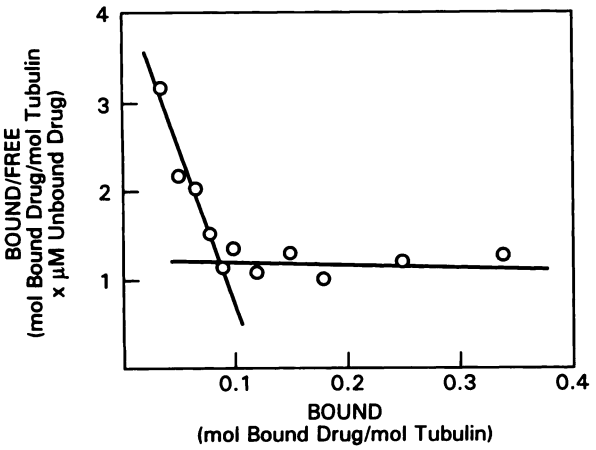

Fig. 3. Scatchard analysis of the binding of [^{3}H]dolastatin 10 to tubulin. Each reaction mixture contained [^{3}H]dolastatin 10 at concentrations ranging from 0.1 to 1.0 μM. Incubation was for 15 min at room temperature. Duplicate 0.15-ml aliquots of each reaction mixture were placed on microcolumns, and centrifugal gel filtration was performed at room temperature. Data averaged from two experiments are presented.

formed (Fig. 3). Note that in this study only substoichiometric (relative to tubulin) drug concentrations were used. A biphasic Scatchard plot was obtained, suggesting two classes of binding sites. The curve representing the apparent high affinity site (obtained from reaction mixtures in which the dolastatin 10 concentration was <0.3 μM) intercepts the abscissa, however, at a stoichiometry of only 0.1. The slope of this curve yields an apparent K_a value of 3.8×10^7 M^{-1} (equivalent to an apparent K_d value of 26 nM). The slope of the curve representing the apparent low affinity site is too shallow for estimation of an apparent K_a value or stoichiometry.

We unsuccessfully attempted to demonstrate binding of superstoichiometric amounts of dolastatin 10 to tubulin, in an effort to obtain direct evidence for two classes of dolastatin 10 binding sites. We examined the binding of drug to tubulin at successively higher drug concentrations (Fig. 4). These studies were performed by column gel filtration at room temperature. In the experiments summarized in Fig. 4, the tubulin concentration in the original reaction mixtures was 2.5 μM, and the dolastatin 10 concentration was 0.5 (Fig. 4A), 2.5 (Fig. 4B), 5 (Fig. 4C), or 10 μM (Fig. 4D). Thus, the tubulin to drug ratio ranged from 0.2 to 4, but the stoichiometry of drug binding rose only from 0.18 mol of dolastatin 10 bound/mol of tubulin in the experiment of Fig. 4A to 0.78 mol/mol in the experiment of Fig. 4D. An additional increase in the [^{3}H]dolastatin 10 concentration to 25 μM (drug:tubulin = 10) yielded no further increase in the amount of dolastatin 10 bound to the protein (0.77 mol/mol). Although we cannot exclude the possibility of drug dissociation from a very low affinity site, with the substoichiometric drug concentration the free drug peak was negligible and the stoichiometry of binding was 90% of the theoretical maximum of 0.2 mol/mol.

Dissociation of dolastatin 10 from tubulin. The experiment shown in Fig. 4 demonstrated that dolastatin 10 bound tightly to tubulin and that isolation of a drug-tubulin complex by gel filtration could be readily accomplished. This was done, and dissociation of radiolabel from protein was negligible unless the tubulin-[^{3}H]dolastatin 10 complex was incubated with an excess of a competing nonradiolabeled drug. In the experiment of Fig. 5A the tubulin-[^{3}H]dolastatin 10 complex (3.4 μM tubulin, bearing 0.63 mol of dolastatin 10/mol of protein) was incubated with an active isomer (isomer 2, see below) of dolastatin 10 at 10 μM, at three temperatures. The results demonstrated a first-order dissociation of radiolabel from protein, with the rate increasing as the temperature rose. The observed half-lives of the tubulin-drug complex and the dissociation rate constants derived from them are summarized in Table 1, and an Arrhenius plot of these data is presented in Fig. 5B. This plot yielded an activation energy for the dissociation reaction of 8.6 kcal/mol.

Tubulin aggregation induced by dolastatin 10. Previously we described apparent dolastatin 10-induced aggregation of tubulin only at high (superstoichiometric) concentrations of drug in the presence of MAPs and GTP (4, 8). Under such conditions the rise in turbidity is irreversible by cold, as are the aggregation reactions induced by the *Vinca* alkaloids (17). These reactions have been advantageously studied by HPLC by Singer and co-workers (18, 19), and we found that

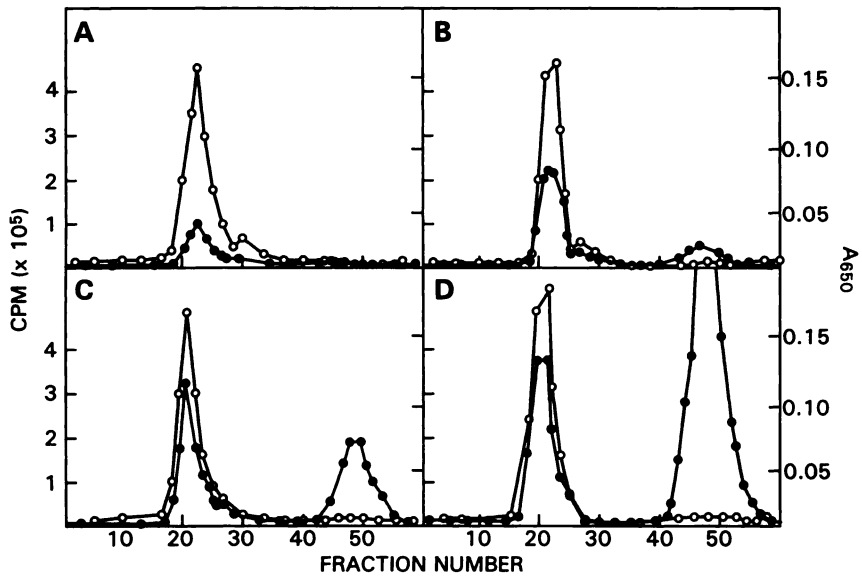

Fig. 4. Quantitation of [^{3}H]dolastatin 10 bound to tubulin by column gel filtration. Reaction mixtures (1.0 ml) contained the following concentrations of [^{3}H]dolastatin 10: A, 0.5 μM; B, 2.5 μM; C, 5.0 μM; D, 10 μM. After a 20-min incubation at room temperature, each reaction mixture was applied to a 1.0- × 25-cm column of Sephadex G-50 (superfine). Chromatography was at room temperature. An aliquot of each fraction was counted in a liquid scintillation counter, and another aliquot was evaluated for protein content by the Lowry procedure. Stoichiometry of binding in the peak protein fractions was as follows: A, 0.18 mol of dolastatin 10/mol of tubulin; B, 0.42 mol/mol; C, 0.69 mol/mol; D, 0.78 mol/mol. ○, A_{650}; ●, radioactivity.

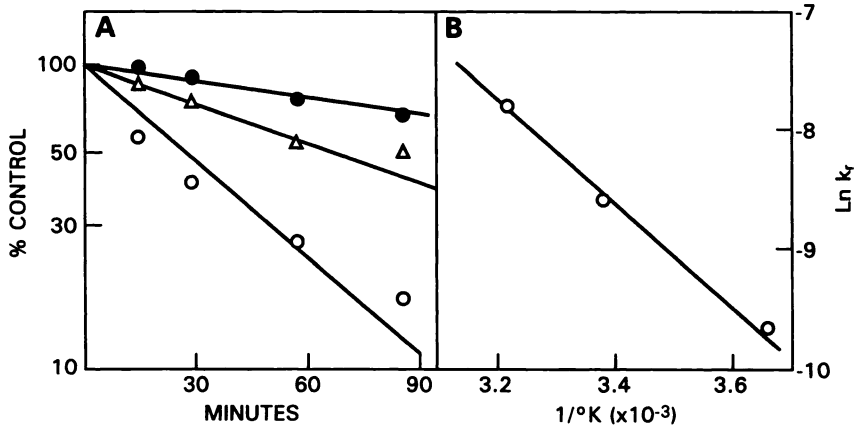

Fig. 5. Dissociation of [^{3}H]dolastatin 10 from tubulin. A, Time course of dissociation at 0° (●), room temperature (△), and 37° (○). The data presented are the average values obtained in three experiments. The tubulin-[^{3}H]dolastatin 10 complex was prepared by incubation of 0.5 mg/ml (5.0 μM) tubulin with 5.0 μM [^{3}H]dolastatin 10 (15-ml reaction mixture) and isolation of the complex on multiple microcolumns of Sephadex G-50 (superfine). The filtrates were pooled, yielding a preparation containing 0.34 mg/ml (3.4 μM) tubulin with 0.63 mol of dolastatin 10/mol of tubulin (average value for the three experiments, representing the unincubated control value). Reaction mixtures (2.0 ml) were prepared from the pool, and 10 μM isomer 2 was added (see Table 2 for structural details). The mixtures were incubated at the indicated temperatures, and at each time point duplicate aliquots were removed and processed by centrifugal gel filtration. For the 37° experiments, the microcolumns were warmed in a water bath, and the centrifuge was at room temperature. For the 0° experiments, incubation was in an ice bath, and centrifugal gel filtration was in a 4° cold room. Without the addition of isomer 2 there was negligible dissociation of dolastatin 10 from tubulin over the time period evaluated. B, Arrhenius plot of the rate constants derived from the data of A (see Table 1).

TABLE 1

Apparent dissociation rate constants for dolastatin 10 dissociation from tubulin

Dissociation rate constants were determined from the data presented in Fig. 5A, which represent average values obtained in three independent experiments, using the formula $k_r = \ln 2/t_{½}$.

Temperature	k_r	$t_{½}$
	sec^{-1}	min
0°	6.4×10^{-5}	180
23°	1.9×10^{-4}	62
37°	4.1×10^{-4}	28

we could apply this technique to other *Vinca* domain drugs (Fig. 6).[1]

Fig. 6A demonstrates the pattern obtained when tubulin alone was injected onto the column, which was then subjected to elution with 0.1 M MES/0.5 mM $MgCl_2$. A small peak emerged in the void volume at about 5.5 min (perhaps representing denatured protein), but the bulk of the tubulin eluted at about 7.7 min (α/β-dimer) as a symmetrical peak. In contrast, with 100 μM vinblastine (Fig. 6B) only a broad peak of aggregate was observed, with its leading edge in the void volume. Fig. 6, C–F, demonstrates the gradual conversion of the α/β-dimer peak to increasing amounts of larger (void volume) and smaller (included peaks) aggregates as the original dolastatin 10 concentration was increased from 0.1 to 1.0 μM. Note that even with a dolastatin 10 concentration as low as 0.1 μM a small included aggregate peak was formed. Fig. 6G demonstrates the complete conversion of α/β-dimer to excluded aggregate with 5 μM dolastatin 10. Fig. 6, H–L, documents the nearly identical effects of phomopsin A on tubulin aggregation at the same concentrations (see Ref. 20).

The finding that dolastatin 10 induced an aggregation reaction raises the question of what tubulin species actually binds the drug. This was investigated by examining reaction

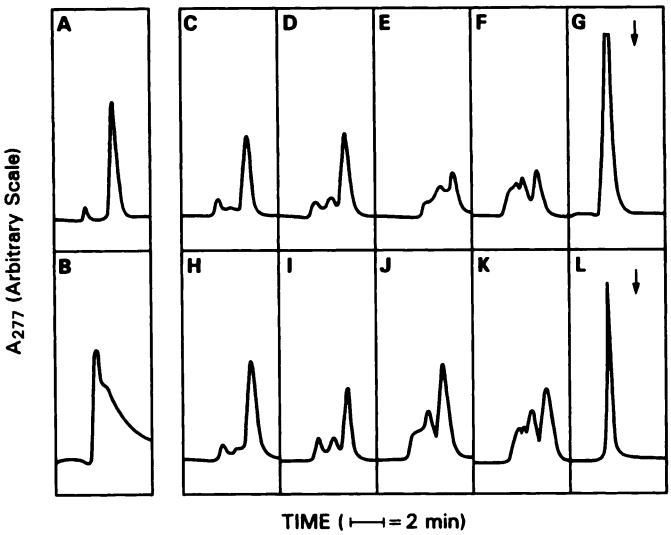

Fig. 6. Drug-induced aggregation of tubulin. Reaction mixtures contained drug as indicated. Incubation was for 20 min at room temperature, and HPLC analysis (LKB system) was performed at room temperature. The injection volume was 0.5 ml, and the flow rate was 1.0 ml/min. A, No drug; B, 100 μM vinblastine; C, D, E, F, and G, 0.1, 0.25, 0.5, 1.0, and 5.0 μM dolastatin 10, respectively; H, I, J, K, and L, 0.1, 0.25, 0.5, 1.0, and 5.0 μM phomopsin A, respectively. The average retention time for the void volume peak was 5.5 min and that for the tubulin dimer peak was 7.7 min. *Arrows in G and L*, expected position of the tubulin heterodimer peak.

mixtures containing radiolabeled dolastatin 10 in an HPLC system equipped with an isotope flow detector (Fig. 7). Fig. 7A again shows the small amount of aggregate observed without drug, and Fig. 7C documents that 5 μM [^{3}H]dolastatin 10, like the nonradiolabeled drug, completely drove the tubulin into an aggregate eluting in the void volume. Not surprisingly, the aggregate peak was heavily radiolabeled and, in accord with the absorbance data, no radiolabeled dolastatin 10 eluted at the position of the tubulin α/β-dimer (Fig. 7C, *arrow*; about 14 min). Excess unbound [^{3}H]dolasta-

[1] In contrast to Singer and co-workers (18, 19), however, we have not included drugs in the buffer solution used to equilibrate and develop the HPLC column.

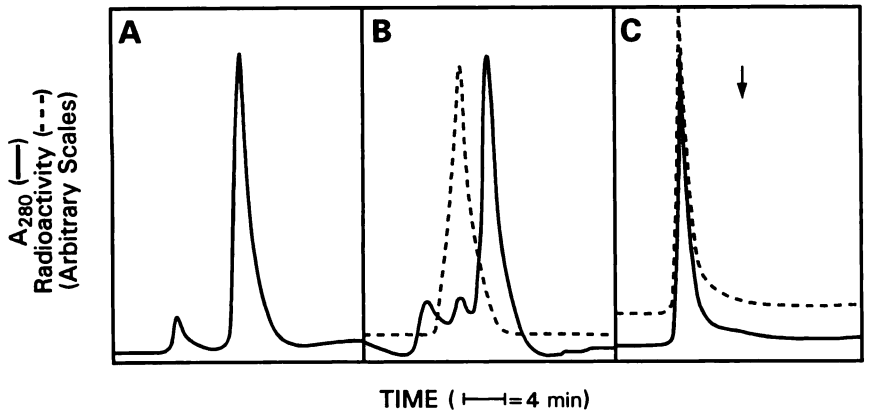

Fig. 7. Association of [^{3}H]dolastatin 10 with aggregated tubulin. Reaction mixtures contained drug as indicated. Incubation was for 20 min at room temperature, and HPLC analysis (Waters system) was performed at room temperature. The injection volume was 0.5 ml, and the flow rate was 0.5 ml/min. A, No drug; B, 0.1 μM [^{3}H]dolastatin 10; C, 5.0 μM [^{3}H]dolastatin 10. The average retention time for the void volume peak was 8.9 min, that for the 200-kDa peak was 11.7 min, and that for the tubulin heterodimer peak was 13.8 min. *Arrow in C*, expected position of the tubulin heterodimer peak.

TABLE 2

Effects of dolastatin 10 and related compounds on tubulin-dependent reactions

For positions in dolastatin 10, see Fig. 1. For the structures of analog 1, tripeptides A and D, and tetrapeptide A, see Fig. 1. Configurations are listed only for positions at which isomeric forms exist. Details are presented for all positions for dolastatin 10. For other compounds, only variations from the dolastatin 10 configuration are listed. For the tripeptides and tetrapeptide, position numbers refer to the analogous positions in dolastatin 10. In analog 1 the substituent at position C10 is absent and the 9–10 bond is unsaturated. For structures of dolastatin 15 and phomopsin A, see Ref. 8. Inhibition of [^{3}H]dolastatin 10 binding was measured by centrifugal gel filtration after a 15-min incubation at room temperature. Reaction mixtures contained 0.25 mg/ml (2.5 μM) tubulin, 2.5 μM [^{3}H]dolastatin 10, and potential inhibitors (including nonradiolabeled dolastatin 10) as indicated. Formation of tubulin aggregates was measured by HPLC as described in the legend to Fig. 7. Reaction mixtures contained 0.25 mg/ml (2.5 μM) tubulin and drug as indicated. The IC_{50} values for inhibition of polymerization, [^{3}H]vinblastine binding, and nucleotide exchange are taken from previous reports (2–4, 7). The value for inhibition of vinblastine binding by phomopsin A is in parentheses because it has not been directly measured. We have, however, directly compared phomopsin A with dolastatin 10 as an inhibitor of [^{3}H]vincristine binding (2), and the value for phomopsin A was twice that for dolastatin 10. For this comparison we are assuming that the two drugs would have a similar relationship for vinblastine binding. [^{3}H]D10, [^{3}H]dolastatin 10; NA, not applicable; NI, not inhibitory.

Peptide	Configuration at position						Inhibition of [^{3}H]D10 binding		Tubulin in void volume (aggregation)		Inhibition of polymerization, IC_{50}	Inhibition of vinblastine binding, IC_{50}	Inhibition of nucleotide exchange, IC_{50}
	6	9	10	18	19	19a	1:1	10:1	5 μM Drug	25 μM Drug			
							%		%		μM	μM	μM
Dolastatin	S	R	R	R	S	S	24	72	100		1.2	6	10
Isomer 1			S				0	1		11	1.3	80	50
Isomer 2						R	69	86	100		1.4	4	7
Isomer 3		S				R	2	0		14	1.2	75	120
Isomer 4		S	S				0	0		12	1.4	120	90
Isomer 5		S					0	0		13	2.6	105	50
Isomer 6				S			0	0		10	10	NI	NI
Isomer 7				S	R		0	0		12	18	NI	NI
Isomer 19	R						10	38	100		1.9	8	7
Analog 1		NA	NA				0	0		13	4.9	140	290
Tripeptide A	NA	NA	NA				0	0		12	4.2	NI	NI
Tripeptide D							0	0		10	13	NI	NI
Tetrapeptide A							0	0		10	3.0	150	230
Phomopsin A							65	96	100		1.4	(12)	5
Dolastatin 15							0	4		10	23	NI	NI

tin 10 eluted at a later time point (about 30 min) (data not shown).

At lower concentrations of [^{3}H]dolastatin 10, where there was residual tubulin α/β-dimer and included oligomer peaks, the peak of radiolabel was always shifted to an earlier time point than the tubulin α/β-dimer peak, even when the [^{3}H]dolastatin 10 was entirely contained within the included volume. The pattern obtained with the lowest concentration of [^{3}H]dolastatin 10 examined (0.1 μM) is shown in Fig. 7B. The radiolabel peak coincided with the small included oligomer peak.[2] In a separate experiment, we found that [^{3}H]dolastatin 10 did not bind to a 200-kDa standard (amylase) and that, when 2.5 μM tubulin, 0.1 μM [^{3}H]dolastatin 10, and the 200-kDa standard were mixed, radiolabel eluted from the column in the same position as the amylase. This indicates that the included oligomer peak contains two α/β-tubulin molecules bound to [^{3}H]dolastatin 10 (see below).

Further information on the interrelationship of the binding of dolastatin 10 to tubulin and its induction of tubulin aggregation was sought by studying chiral isomers (isomers 1–7 and isomer 19), segments (tripeptides A and D and tetrapeptide A), and a dolastatin 10 analog active as inhibitors of polymerization (7, 13) (for structural details, see Fig. 1 and Table 2). These compounds, as well as dolastatin 15 and phomopsin A, were examined for inhibitory effects on the binding of [^{3}H]dolastatin 10 to tubulin and for their own abilities to induce aggregation reactions. Table 2 summarizes these new findings and compares them with previously ob-

[2] Note that there is modest slurring in the trailing edge of the radiolabel peak in Fig. 7B. This could represent some binding (5–10%) of [^{3}H]dolastatin 10 to α/β-dimer or some dissociation of drug from protein under the nonequilibrium chromatography conditions.

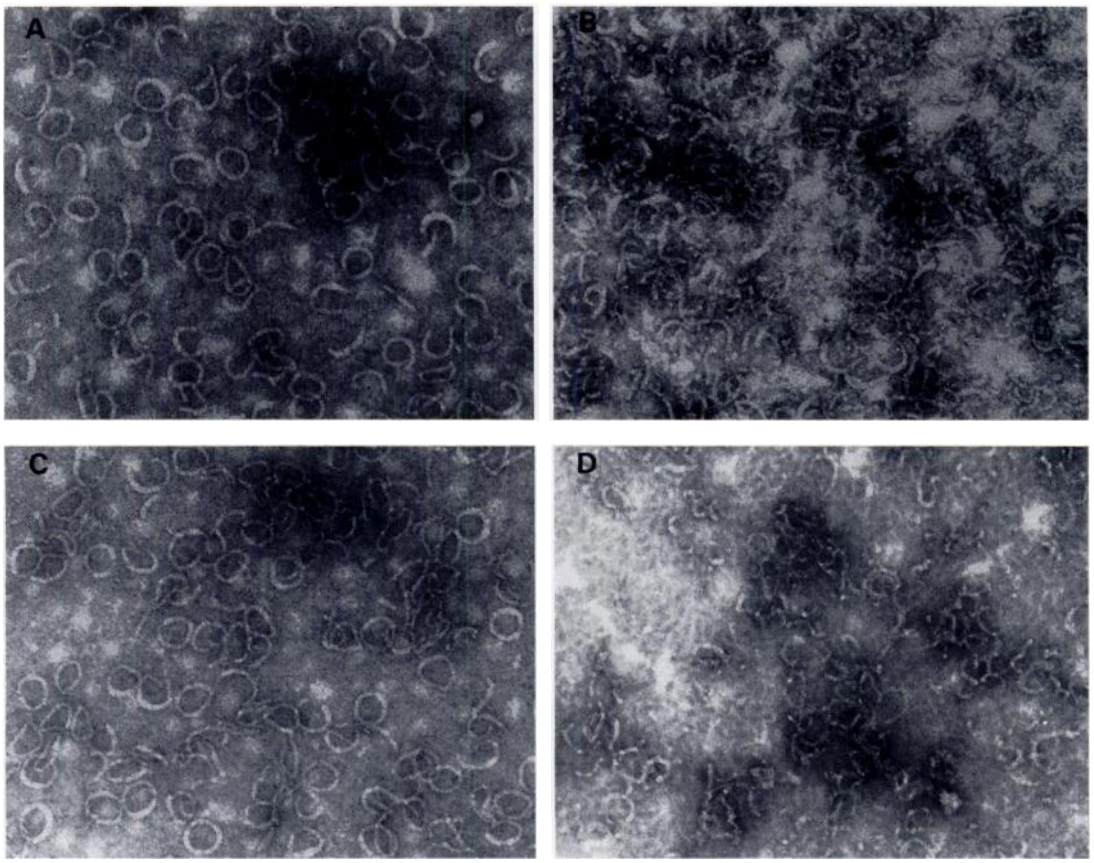

Fig. 8. Comparison of the morphology of dolastatin 10-induced aggregates (A and C) and vinblastine-induced aggregates (B and D) in the absence of MAPs. All reaction mixtures contained MES and $MgCl_2$, as described in the text, plus drug at 20 μM. When present (C and D), the GTP concentration was 0.2 mM. The drug was always the last component added to the reaction mixture. A, B, and C, The reaction mixtures contained tubulin at 0.25 mg/ml and were incubated at room temperature before grid preparation. D, The reaction mixture contained tubulin at 1.0 mg/ml, and the grid was prepared after the 37° incubation (see text). Magnification, 103,000×.

tained results with these agents as inhibitors of polymerization, vinblastine binding, and nucleotide exchange.

Only phomopsin A and two chiral isomers (isomers 2 and 19) significantly inhibited binding of [^{3}H]dolastatin 10 to tubulin, with phomopsin A and isomer 2 being more effective than nonradiolabeled dolastatin 10 as an inhibitor and isomer 19 being less effective than dolastatin 10. Besides dolastatin 10 and phomopsin A (Fig. 6L), only isomers 2 and 19 at 5 μM were able to cause total formation of large (void volume) tubulin aggregates. The remaining isomers and the segments and analog, as well as dolastatin 15, were unable to induce formation of large aggregates even at 25 μM. Some broadening of the heterodimer peak or appearance of small included aggregate peaks was observed with several of the less active compounds at 25 μM (isomers 1, 3, 4, 5, and 7 and analog 1) (data not shown).

Morphology of dolastatin 10-induced aggregates. We have examined dolastatin 10-induced aggregates by electron microscopy under a variety of reaction conditions, including different drug and tubulin concentrations, and after incubations at room temperature (as was used in the HPLC studies described above) or 37°. Simultaneous studies were performed with vinblastine for comparison. Neither the concentration of drug or tubulin nor the reaction temperature had a major impact on the morphology of the aggregates, except for the apparent size of clusters visualized on the grids (significantly larger at higher tubulin concentrations). Significant morphological changes occurred when MAPs were included in the reaction mixture. GTP (always added before drug addition to minimize inhibition of GTP binding to tubulin) had little effect on aggregate morphology with either dolastatin 10 or vinblastine.[3]

Typical high-power views are presented in Figs. 8 (without MAPs) and 9 (with MAPs), comparing aggregate formed with dolastatin 10 with aggregate formed with vinblastine. The aggregates formed when the only components (besides MES and $MgCl_2$) in the reaction mixtures were tubulin and drug (reaction conditions comparable to those used in the HPLC studies) are shown in Fig. 8, A and B. The dolastatin 10 aggregate (Fig. 8A) appeared to be composed primarily of single rings, filamentous fibers that may represent broken rings, and areas of clustered rings that suggest an underlying substructure of tightly coiled spirals. Thus far we have not obtained a well defined image of the vinblastine aggregate (Fig. 8B), which appeared to consist of short disorganized

[3] A few observations have been made of samples without drug. No morphologically distinct aggregates were observed with tubulin or tubulin plus GTP. With MAPs and no GTP, scattered separated rings and short filaments were observed in a sample taken from a reaction mixture at 0°. These persisted in the reaction mixture when it was warmed first to room temperature and then to 37°. Addition of GTP to the reaction mixture appeared to increase the amount of rings and filaments at 0°. When this reaction mixture was warmed successively to room temperature and 37°, the rings disappeared and a few microtubules appeared (at room temperature). At 37°, abundant microtubules formed.

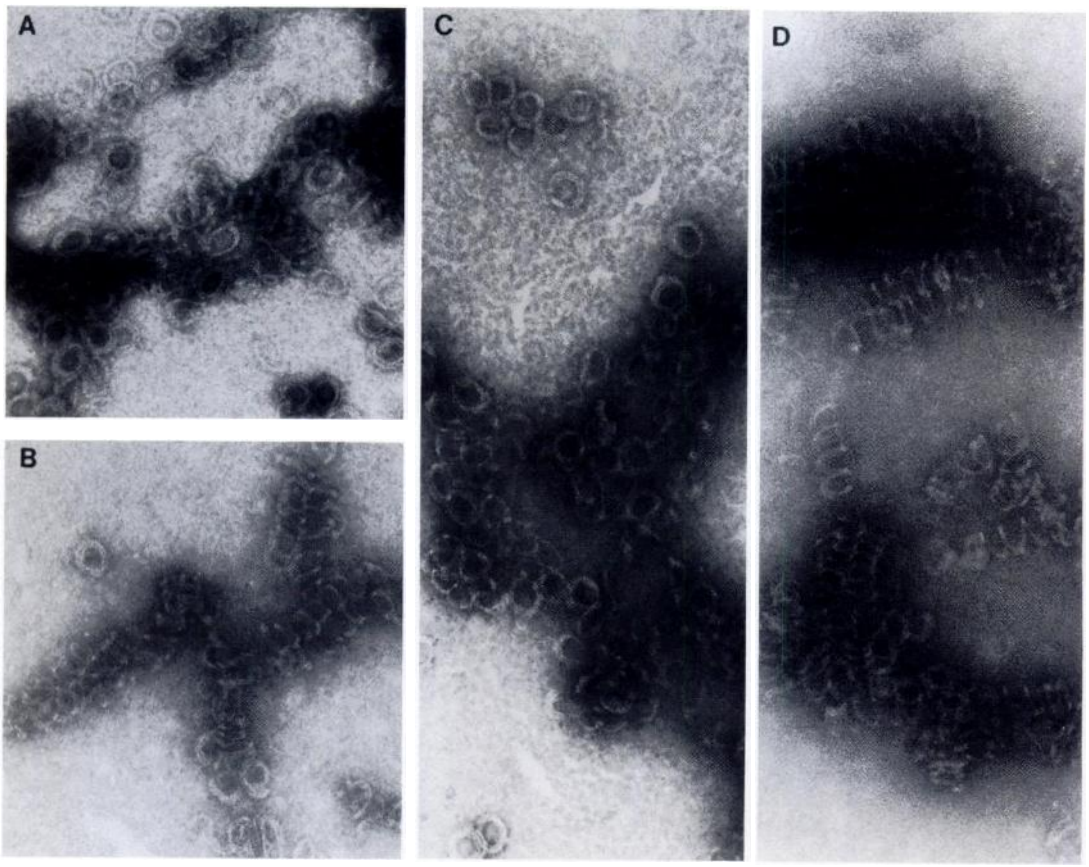

Fig. 9. Comparison of the morphology of dolastatin 10-induced aggregates (A and C) and vinblastine-induced aggregates (B and D) in the presence of MAPs. All reaction mixtures contained MES and $MgCl_2$, as described in the text, plus drug at 20 μM. When present (C and D), the GTP concentration was 0.2 mM. The drug was always the last component added to the reaction mixture. A and C, The reaction mixtures contained tubulin at 1.0 mg/ml and MAPs at 0.5 mg/ml; B and D, the reaction mixtures contained tubulin at 0.25 mg/ml and MAPs at 0.13 mg/ml. A, B, and D, Grids were prepared after the room temperature incubation; C, the grid was prepared after the 37° incubation (see text). Magnification, 102,000×.

filaments. Addition of GTP to the reaction mixtures (Fig. 8, C for dolastatin 10 and D for vinblastine) had little effect on the morphology observed with either drug.

When heat-treated MAPs were added to the reaction mixture, whether or not GTP was also added, the aggregate fine structures with both drugs had a much more highly organized appearance than without MAPs (Fig. 9). With dolastatin 10 (Fig. 9, A, no GTP, and C, with GTP) the initial impression was of interconnecting rings everywhere, with single and isolated adjacent rings at the fringes of the aggregate mass. With vinblastine (Fig. 9, B, no GTP, and D, with GTP) fine structure was most readily visible at the edges of dense aggregates. In agreement with the findings of many workers (reviewed in Ref. 17), we found that the drug induced formation of tight spirals of indefinite length, although a few rings were also seen.

Closer observation of the aggregate induced by dolastatin 10 (with MAPs) revealed sporadic areas (Fig. 10A) where what appear to be oblique (Fig. 10A, *arrow*) and lateral views of the rings were visualized. These suggest that the underlying structure of the dolastatin 10/MAPs aggregate is a coiled spiral, probably tighter than that induced by vinblastine (Fig. 9, B and D). The prominent ring appearance of the aggregate could therefore result either from the bulk of the aggregate consisting of relatively short coils or from its being relatively fragile and fragmenting during specimen preparation. Very high-power views of short coils viewed laterally are shown in Fig. 10, B and C (*arrows*).

The most morphologically distinct aggregate induced by dolastatin 10 resembles a pinwheel, as shown in very high-power views in Fig. 11. These structures were observed only when MAPs were included in the reaction mixture, but they were present both with and without GTP. Occasionally a pinwheel structure was found intermingled, perhaps continuous with, the more typical interconnecting rings (Fig. 11A), but the pinwheels were more often found almost completely isolated from other aggregates. Partial pinwheels were relatively common, sometimes appearing continuous with poorly defined filaments (Fig. 11B). Occasionally, however, nearly perfect and complete pinwheels were observed (Fig. 11, C and D). These structures have thus far not been observed in the absence of MAPs or after incubation with vinblastine. They have, however, been observed in reaction mixtures containing MAPs and phomopsin A (8) (see also Ref. 9 for morphologically similar structures formed when phomopsin A was added to microtubules formed from microtubule protein).

Discussion

Interpretation of apparent rate and equilibrium constants. The interaction of [^{3}H]dolastatin 10 with tubulin is not simple, and description of this interaction requires

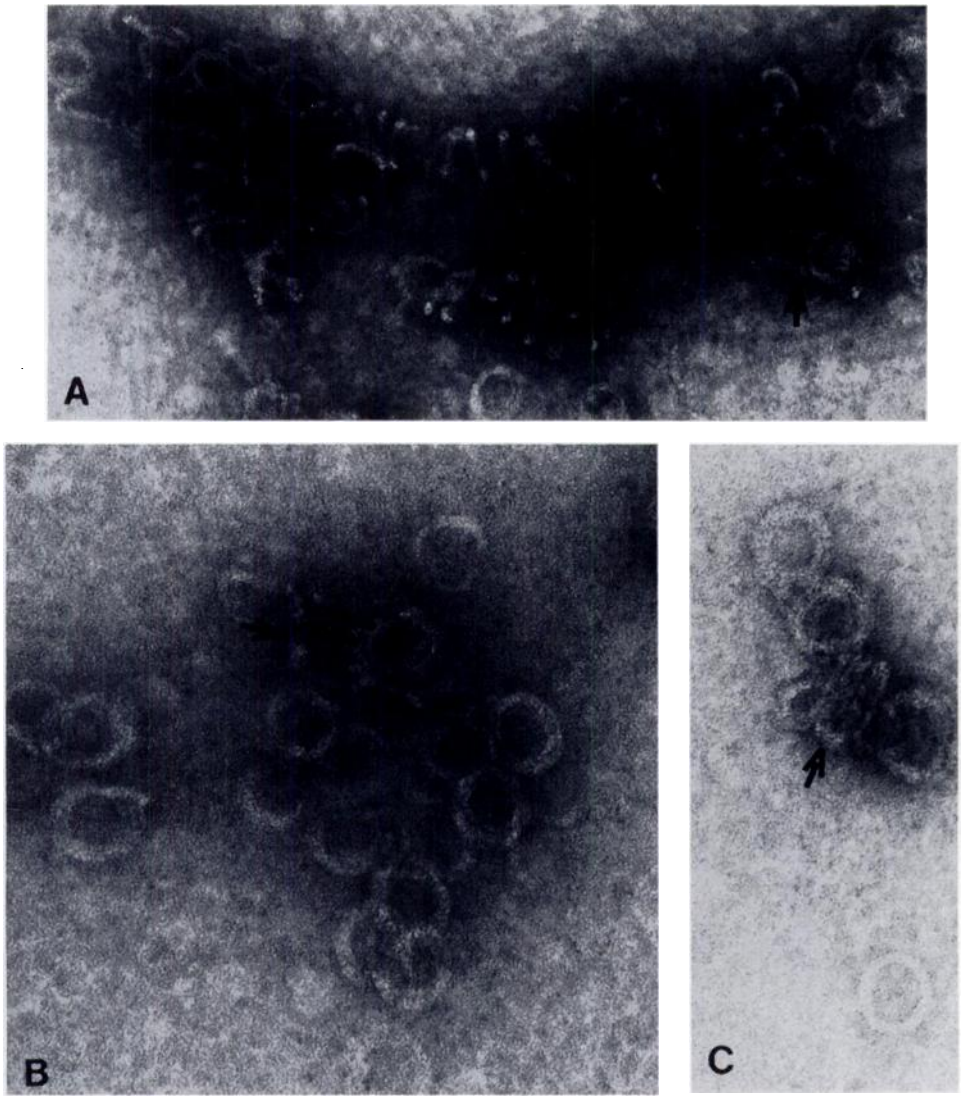

Fig. 10. Coil aggregates induced by dolastatin 10 in the presence of MAPs. The reaction mixtures were prepared as described for the sample presented in Fig. 9C, except that the sample presented in A contained 40 μM dolastatin 10. Magnifications: A, 145,000×; B and C, 249,000×. *Arrow in A*, what appears to be an obliquely visualized coil; *arrows in B and C*, short tight coils.

consideration of the tubulin aggregation reaction caused by the drug. The Scatchard analysis (Fig. 3) of dolastatin 10 binding was biphasic, as has been observed with *Vinca* alkaloids (17, 21–24) and phomopsin A (20). In an elegant analysis Timasheff and colleagues (23–25) argued persuasively that the biphasic pattern routinely observed with *Vinca* alkaloids is derived from aggregation reactions that follow drug binding to a single high affinity site, rather than from two classes of drug binding sites. The same analysis should apply to the biphasic patterns that occur with phomopsin A, as described by Li *et al.* (20), and with dolastatin 10 reported here.

In this analysis the high affinity Scatchard binding constant is derived from a simple protein-drug interaction:

$$\text{Tubulin} + \text{dolastatin 10} \underset{k_r}{\overset{k_f}{\rightleftarrows}} \text{tubulin-dolastatin 10 complex} \quad (1)$$

The data of Fig. 3 yielded an association constant of 3.8×10^7 M^{-1} at room temperature. Ignoring the effects of tubulin-aggregation on the dissociation of [^{3}H]dolastatin 10 in the presence of isomer 2, the data of Fig. 5 yield a value of 1.9×10^{-4} sec^{-1} for k_r at room temperature. Because

$$k_f = K_a \times k_r \quad (2)$$

the value of k_f at room temperature would be 7.2×10^3 M^{-1} sec^{-1}.

We can determine whether this derived value of k_f is reasonable. From Fig. 2 it seems likely that at room temperature the time 0 value would be intermediate between those obtained by placing the samples on cold and warm microcolumns. Arbitrarily taking a value between the two experimental values (about 0.026 mol of bound drug/mol of tubulin) and assuming that half of this binding would have occurred at a reasonably linear rate, one can calculate a reaction time using the derived k_f. Such a calculation yields a reaction time of 11 sec, which seems reasonable.

Nevertheless, we must emphasize that both the k_r and K_a values obtained experimentally are tentative, because of the associated dolastatin 10-induced aggregation reactions. Measurement of the k_r values required that an alternate drug with high affinity for tubulin at the dolastatin 10 site be used to prevent rebinding of [^{3}H]dolastatin 10. All such agents themselves cause aggregation reactions, including isomer 2,

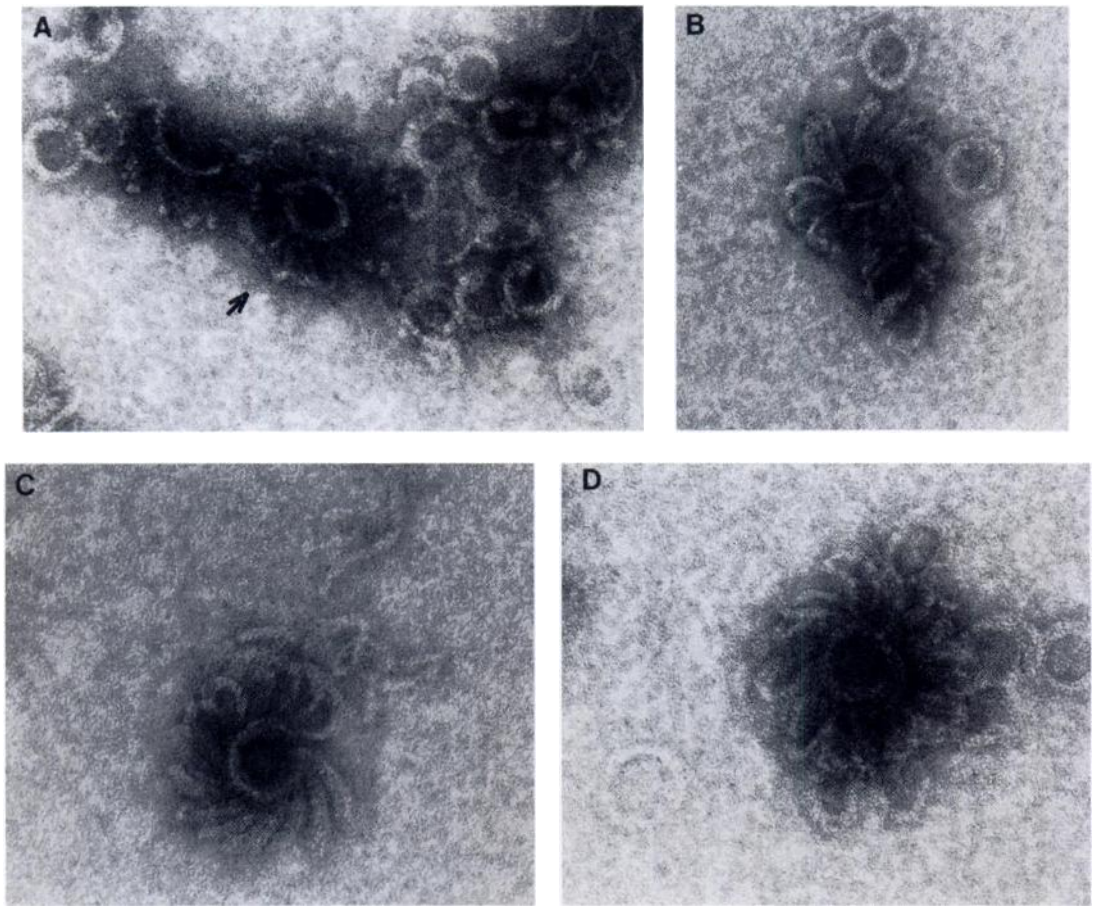

Fig. 11. Pinwheel aggregates induced by dolastatin 10 in the presence of MAPs. The reaction mixtures were prepared as described for the sample presented in Fig. 9C. Magnifications: A and B, 186,000×; C and D, 233,000×. *Arrow in A*, pinwheel aggregate apparently conjoined to aggregates with other morphologies.

which was used in the studies of Fig. 5. The apparent values for k_r may thus be incorrect, not only because disaggregation reactions (not drug dissociation) may be the rate-limiting steps but also because it is possible that radiolabel may be directly displaced in the aggregates in the presence of an alternate active drug.

The major problem with the Scatchard-derived K_a value is that our data indicate that, even at the lowest drug concentrations used, we are measuring binding of [^{3}H]dolastatin 10 to small aggregates (Fig. 7B). The slope obtained from the Scatchard data thus probably represents a complex value rather than a true equilibrium constant for the association of dolastatin 10 with tubulin heterodimer.

The actual identity of the small oligomer identified in the study presented in Fig. 7B is at present unknown. It seems unlikely to represent simply a conformational change in the tubulin-dolastatin 10 complex, and its comigration with a 200-kD standard indicates that it contains two tubulin heterodimers. The minimum composition of this complex would be two tubulin molecules and one molecule of dolastatin 10 (tubulin-dolastatin 10-tubulin complex) or, depending on the relative stability of aggregates, two tubulin molecules liganded to two dolastatin 10 molecules (tubulin-dolastatin 10-tubulin-dolastatin 10 complex). The relative protein content of this small peak suggests that it is a tubulin-dolastatin 10-tubulin-dolastatin 10 complex. In the control without drug, about 10% of the protein appears in the void volume, probably representing denatured aggregate. Because with substoichiometric concentrations of [^{3}H]dolastatin 10 virtually all drug binds to tubulin (Fig. 4), with 0.1 μM drug plus 2.5 μM tubulin (90% active) a tubulin-dolastatin 10-tubulin-dolastatin 10 peak should contain about 4.5% of the protein, whereas a tubulin-dolastatin 10-tubulin peak should contain about 9% of the protein. The relative size of the radiolabeled peak (from the absorbance tracing) in Fig. 7B is more consistent with the former than the latter. One possible pathway to such a complex,

$$T + D \underset{}{\overset{\text{slow}}{\rightleftarrows}} T{-}D \overset{\text{fast}}{\rightleftarrows} T{-}D{-}T \overset{\text{fast}}{\underset{\text{slow}}{\rightleftarrows}} T{-}D{-}T{-}D \qquad (3)$$

where T is tubulin and D is dolastatin 10, suggests that the Scatchard analysis yields an apparent K_a value representing a blend of the initial association rate constant and the third dissociation rate constant.

Dolastatin 10 binding site. Earlier experiments with radiolabeled vinblastine and vincristine yielded noncompetitive patterns of inhibition by dolastatin 10 and phomopsin A versus competitive patterns for maytansine and rhizoxin, as well as the alternate *Vinca* alkaloid (4, 5). This led us to propose that the actual binding site for the peptide antimitotics differed from that of vinblastine/maytansine/rhizoxin.

We proposed that the two sites were physically close

together on the tubulin molecule, in a region we called the *Vinca* domain, to account for the significant overlap in the biochemical properties of the two groups of drugs. Among the peptide antimitotic natural products and related synthetic peptides, there seem to be concordant effects on all biochemical properties, except for inhibition of tubulin polymerization (Table 2; see also Ref. 7). Thus, strong peptide inhibitors of vinblastine binding also inhibit dolastatin 10 binding and nucleotide exchange, readily induce aggregate formation (Table 2), and stabilize tubulin conformation (7). However, this concordance does not persist when other *Vinca* domain agents are considered. For example, maytansine strongly inhibits vinblastine (5, 26, 27) and dolastatin 10 binding to tubulin and nucleotide exchange (4, 28), but maytansine neither stabilizes tubulin conformation nor induces tubulin aggregation (4, 27, 29, 30). Vinblastine, while inducing aggregation, only partially stabilizes tubulin conformation (29, 31) and only minimally affects nucleotide exchange (4, 28) and dolastatin 10 binding. In contrast, rhizoxin fits rather well into the pattern observed with the peptides, because it does not cause tubulin aggregation (32, 33), does not stabilize the conformation of tubulin (4, 34), and is relatively weak as an inhibitor of nucleotide exchange and of *Vinca* alkaloid (4, 5) and dolastatin 10 binding.[4]

The comparison of morphological effects of dolastatin 10 and vinblastine on tubulin aggregates provides additional evidence that two distinct binding sites may be involved in their interactions with tubulin. The aggregates induced by the two drugs are structurally distinct, presumably caused by interactions at different sites on the protein. Spiral structures, perhaps related to protofilaments, were induced by both drugs. These appear to be more tightly coiled in the presence of dolastatin 10 than of vinblastine, especially in the presence of MAPs, leading to the appearance of adjacent and interconnecting rings with the peptide and more obvious spirals with vinblastine. Most notably, a striking "pinwheel" fragment was observed with dolastatin 10 but not with vinblastine in the presence of MAPs.

It is also worth reiterating the similarities we have found between dolastatin 10 and phomopsin A, although a major difference between the two peptides is that phomopsin A is >10,000-fold less toxic to cells growing in culture (2). Both peptides show noncompetitive patterns of inhibition versus radiolabeled vincristine, stabilize colchicine binding, and strongly inhibit nucleotide exchange (4). Both induce pinwheel tubulin aggregates in the presence of MAPs (8) (Fig. 11) and have nearly identical quantitative effects on the formation of small tubulin aggregates without MAPs, as measured by HPLC (Fig. 6). In initial experiments we have also obtained a competitive pattern of inhibition by phomopsin A of [^{3}H]dolastatin 10 binding to tubulin.[5] Finally, analysis of the binding of [^{3}H]dolastatin 10 to tubulin yielded a biphasic Scatchard plot (Fig. 2), comparable to the result obtained by Li *et al.* (20) with radiolabeled phomopsin A. We should note, however, that Li *et al.* have been unable to demonstrate aggregate formation with phomopsin A (20, 35) but observed aggregate formation with dolastatin 10, which they also found strongly inhibited the binding of radiolabeled rhizoxin and phomopsin A to tubulin (35).

Besides the HPLC and electron micrographic evidence for dolastatin 10-induced aggregation of tubulin, we should note that dolastatin 10 causes a marked increase in turbidity of tubulin solutions, even at 0°, which is apparent to the unaided eye. These aggregation reactions are strongly inhibited by spongistatin 1,[6] a highly potent *Vinca* domain drug (36). We found that progressively higher concentrations of spongistatin 1 were required to inhibit turbidity development, aggregation products visualized by electron microscopy, and aggregation products detected by HPLC. This probably reflects increases in sensitivity for progressively smaller aggregates with these three techniques. We estimate that the void volume peak in HPLC contains aggregates as small as four or five α/β-dimers, and only at a ratio of dolastatin 10/phomopsin A to tubulin of 0.4:1 (Fig. 6, F and K) was a peak intermediate between the void volume and the presumptive 200-kDa peak observed (presumably a trimer).

In summary, radiolabeled dolastatin 10 was prepared and its interactions with tubulin were studied. Biphasic results were obtained when drug binding was analyzed by the Scatchard method and when the time course of binding was followed. This probably results from aggregate formation induced by dolastatin 10. Although binding was reversible, in that [^{3}H]dolastatin 10 could be displaced from tubulin by an active isomer, we could not demonstrate binding of drug to tubulin dimer. The smallest species in which radiolabeled drug could be detected appeared to be a small oligomer consisting of two molecules each of tubulin and dolastatin 10. Under most reaction conditions the dolastatin 10-induced aggregate had the appearance of adjacent and interconnected rings that probably were tight spirals. Their appearance usually differed from that of vinblastine-induced aggregate, which generally consisted of more well defined spirals.

Acknowledgments

The authors thank J. F. Endlich for assistance with the electron microscopy.

References

1. Pettit, G. R., Y. Kamano, C. L. Herald, A. A. Tuinman, F. E. Boettner, H. Kizu, J. M. Schmidt, L. Baczynskyj, K. B. Tomer, and R. J. Bontems. The isolation and structure of a remarkable marine animal antineoplastic constituent: dolastatin 10. *J. Am. Chem. Soc.* **109**:6883–6885 (1987).
2. Bai, R., G. R. Pettit, and E. Hamel. Dolastatin 10, a powerful cytostatic peptide derived from a marine animal: inhibition of tubulin polymerization mediated through the *Vinca* alkaloid binding domain. *Biochem. Pharmacol.* **39**:1941–1949 (1990).
3. Bai, R., S. J. Friedman, G. R. Pettit, and E. Hamel. Dolastatin 15, a potent antimitotic depsipeptide derived from *Dolabella auricularia*: interaction with tubulin and effects on cellular microtubules. *Biochem. Pharmacol.* **43**:2637–2645 (1992).
4. Bai, R., G. R. Pettit, and E. Hamel. Binding of dolastatin 10 to tubulin at a distinct site for peptide antimitotic agents near the exchangeable nucleotide and *Vinca* alkaloid sites. *J. Biol. Chem.* **265**:17141–17149 (1990).
5. Bai, R., K. D. Paull, C. L. Herald, L. Malspeis, G. R. Pettit, and E. Hamel. Halichondrin B and homohalichondrin B, marine natural products binding in the *Vinca* domain of tubulin: discovery of tubulin-based mechanism of action by analysis of differential cytotoxicity data. *J. Biol. Chem.* **266**: 15882–15889 (1991).
6. Ludueña, R. F., M. C. Roach, V. Prasad, and G. R. Pettit. Interaction of dolastatin 10 with bovine brain tubulin. *Biochem. Pharmacol.* **43**:539–543 (1992).
7. Bai, R., M. C. Roach, S. K. Jayaram, J. Barkoczy, G. R. Pettit, R. F.

[4] Inhibitory effects of drugs on the binding of dolastatin 10 to tubulin will be described in detail elsewhere.

[5] R. Bai, unpublished observations.

[6] Bai, R., G. F. Taylor, Z. A. Cichacz, C. L. Herald, J. A. Kepler, G. R. Pettit, and E. Hamel. The spongistatins, potently cytotoxic inhibitors of tubulin polymerization, bind in a distinct region of the *Vinca* domain.

Ludueña, and E. Hamel. Differential effects of active isomers, segments, and analogs of dolastatin 10 on ligand interactions with tubulin: correlation with cytotoxicity. *Biochem. Pharmacol.* **45**:1503–1515 (1993).
8. Hamel, E. Natural products which interact with tubulin in the *Vinca* domain: maytansine, rhizoxin, phomopsin A, dolastatins 10 and 15 and halichondrin B. *Pharmacol. Ther.* **55**:31–51 (1992).
9. Tonsing, E. M., P. S. Steyn, M. Osborn, and K. Weber. Phomopsin A, the causative agent of lupinosis, interacts with microtubules *in vivo* and *in vitro*. *Eur. J. Cell Biol.* **35**:156–164 (1984).
10. Hamel, E., and C. M. Lin. Separation of active tubulin and microtubule-associated proteins by ultracentrifugation and isolation of a component causing the formation of microtubule bundles. *Biochemistry* **23**:4173–4184 (1984).
11. Pettit, G. R., S. B. Singh, F. Hogan, P. Lloyd-Williams, D. L. Herald, D. D. Burkett, and P. J. Clewlow. The absolute configuration and synthesis of natural (−)-dolastatin 10. *J. Am. Chem. Soc.* **111**:5463–5465 (1989).
12. Pettit, G. R., D. L. Herald, S. B. Singh, T. J. Thornton, and J. T. Mullaney. Antineoplastic agents. 220. Synthesis of natural (−)-dolastatin 15. *J. Am. Chem. Soc.* **113**:6692–6693 (1991).
13. Bai, R., G. R. Pettit, and E. Hamel. Structure-activity studies with chiral isomers and with segments of the antimitotic marine peptide dolastatin 10. *Biochem. Pharmacol.* **40**:1859–1864 (1990).
14. Culvenor, C. C. J., P. A. Cockrum, J. A. Edgar, J. L. Frahn, C. P. Gorst-Allman, A. J. Jones, W. F. O. Marasas, K. E. Murray, L. W. Smith, P. S. Steyn, R. Vleggaar, and P. L. Wessels. Structure elucidation of phomopsin A, a novel cyclic hexapeptide mycotoxin produced by *Phomopsis leptostromiformis*. *J. Chem. Soc. Chem. Commun.* 1259–1262 (1983).
15. Hamel, E., and C. M. Lin. Guanosine 5′-*O*-(3-thiotriphosphate), a potent nucleotide inhibitor of microtubule assembly. *J. Biol. Chem.* **259**:11060–11069 (1984).
16. Banerjee, A., and R. F. Ludueña. Distinct colchicine binding kinetics of bovine brain tubulin lacking the type III isotype of β-tubulin. *J. Biol. Chem.* **266**:1689–1691 (1991).
17. Himes, R. H. Interactions of the *Catharanthus* (*Vinca*) alkaloids with tubulin and microtubules. *Pharmacol. Ther.* **51**:257–267 (1991).
18. Singer, W. D., R. T. Hersh, and R. H. Himes. Effect of solution variables on the binding of vinblastine to tubulin. *Biochem. Pharmacol.* **37**:2691–2696 (1988).
19. Singer, W. D., and R. H. Himes. Cellular uptake and tubulin binding properties of four *Vinca* alkaloids. *Biochem. Pharmacol.* **43**:545–551 (1992).
20. Li, Y., H. Kobayashi, Y. Tokiwa, Y. Hashimoto, and S. Iwasaki. Interaction of phomopsin A with porcine brain tubulin: inhibition of tubulin polymerization and binding at a rhizoxin binding site. *Biochem. Pharmacol.* **43**:219–224 (1992).
21. Bhattacharyya, B., and J. Wolff. Tubulin aggregation and disaggregation: mediation by two distinct vinblastine-binding sites. *Proc. Natl. Acad. Sci. USA* **73**:2375–2378 (1976).
22. Safa, A. R., E. Hamel, and R. L. Felsted. Photoaffinity labeling of tubulin subunits with a photoactive analogue of vinblastine. *Biochemistry* **26**:97–102 (1987).
23. Na, G. C., and S. N. Timasheff. Interaction of vinblastine with calf brain tubulin: effects of magnesium ions. *Biochemistry* **25**:6222–6228 (1986).
24. Timasheff, S. N., J. M. Andreu, and G. C. Na. Physical and spectroscopic methods for the evaluation of the interactions of antimitotic agents with tubulin. *Pharmacol. Ther.* **52**:191–210 (1991).
25. Na, G. C., and S. B. Timasheff. Interaction of vinblastine with calf brain tubulin: multiple equilibria. *Biochemistry* **25**:6214–6222 (1986).
26. Mandelbaum-Shavit, F., M. K. Wolpert-DeFilippes, and D. G. Johns. Binding of maytansine to rat brain tubulin. *Biochem. Biophys. Res. Commun.* **72**:47–54 (1976).
27. Bhattacharyya, B., and J. Wolff. Maytansine binding to the vinblastine sites on tubulin. *FEBS Lett.* **75**:159–162 (1977).
28. Huang, A. B., C. M. Lin, and E. Hamel. Maytansine inhibits nucleotide binding at the exchangeable site of tubulin. *Biochem. Biophys. Res. Commun.* **128**:1239–1246 (1985).
29. Prasad, A. R. S., R. F. Ludueña, and P. M. Horowitz. Bis(8-anilinonaphthalene-1-sulfonate) as a probe for tubulin decay. *Biochemistry* **25**:739–742 (1986).
30. Fellous, A., R. F. Ludueña, V. Prasad, M. A. Jordan, W. Anderson, R. Ohayon, and P. T. Smith. Effects of tau and MAP_2 on the interaction of maytansine with tubulin: inhibitory effect of maytansine on vinblastine-induced aggregation of tubulin. *Cancer Res.* **45**:5004–5010 (1985).
31. Ludueña, R. F., V. Prasad, M. C. Roach, and E. Lacey. The interaction of phomopsin A with bovine brain tubulin. *Arch. Biochem. Biophys.* **272**:32–38 (1989).
32. Takahashi, M., S. Iwasaki, H. Kobayashi, S. Okuda, T. Murai, and Y. Sato. Rhizoxin binding to tubulin at the maytansine-binding site. *Biochim. Biophys. Acta* **926**:215–223 (1987).
33. Takahashi, M., S. Iwasaki, H. Kobayashi, and S. Okuda. Studies on macrocyclic lactone antibiotics. XI. Anti-mitotic and anti-tubulin activity of new antitumor antibiotics, rhizoxin and its homologues. *J. Antibiot. (Tokyo)* **40**:66–72 (1987).
34. Sullivan, A. S., V. Prasad, M. C. Roach, M. Takahashi, S. Iwasaki, and R. F. Ludueña. Interaction of rhizoxin with bovine brain tubulin. *Cancer Res.* **50**:4277–4280 (1990).
35. Li, Y., H. Kobayashi, Y. Hashimoto, R. Shirai, A. Hirata, K. Hayashi, Y. Hamada, T. Shioiri, and S. Iwasaki. Interaction of marine toxin dolastatin 10 with porcine brain tubulin: competitive inhibition of rhizoxin and phomopsin A binding. *Chem. Biol. Interact.* **93**:175–183 (1994).
36. Bai, R., Z. A. Cichacz, C. L. Herald, G. R. Pettit, and E. Hamel. Spongistatin 1, a highly cytotoxic, sponge-derived, marine natural product that inhibits mitosis, microtubule assembly, and the binding of vinblastine to tubulin. *Mol. Pharmacol.* **44**:757–766 (1993).

Send reprint requests to: E. Hamel, Building 37, Room 5C25, National Institutes of Health, Bethesda, MD 20892.